

Pilot study on proximal femur strains during locomotion and fall-down scenario

Adam Klodowski · Antti Valkeapää · Aki Mikkola

Received: 15 May 2011 / Accepted: 4 April 2012 / Published online: 5 May 2012
© Springer Science+Business Media B.V. 2012

Abstract The most common and severe type of fracture among the elderly is known as a proximal femur fracture. Aging-related bone loss is one of the major contributing factors to increased likelihood of bone fracture. Specific exercises can be used to strain bones and increase bone strength to counter the effects of bone loss. The flexible multibody simulation approach can be used as a non-invasive method for estimating bone strains caused by physical activity. This method was recently used to analyze the strain of locomotion in regard to human femur and tibia leg bones. The current study focuses on strain analysis of the femoral neck. The research test person was a clinically healthy 65-year old Caucasian male. The computed tomography was used to build a geometrically accurate finite element model of the femur with inhomogeneous material properties derived from the voxel data. The anthropometric data was used to model the musculoskeletal system of the test person. The multibody skeletal model was utilized to estimate loading on the femoral neck during walking, which represents a routine daily activity. The flexible multibody simulation results were compared to strains that occurred during a simulated fall onto the greater trochanter of the femur. The fall simulation was made entirely using finite element software. Results from the finite element analysis were compared with the previous study showing that the test person does not belong to the high-risk hip fracture group. Finally, the estimated strains gathered from the walking simulation were compared to the strain values from the simulated fall-down scenario.

Keywords Finite element method · Computed tomography · Biomechanics · Gait

A. Klodowski (✉) · A. Valkeapää · A. Mikkola
Lappeenranta University of Technology, Skinnarilankatu 34, 53850 Lappeenranta, Finland
e-mail: adam.klodowski@lut.fi

A. Valkeapää
e-mail: antti.valkeapaa@lut.fi

A. Mikkola
e-mail: aki.mikkola@lut.fi

1 Introduction

Osteoporosis is a serious health problem, manifesting itself as bone fragility. According to European statistics [1] it affects around 33 % of postmenopausal women and around 20 % of elderly men. It is an inconspicuous disease since it does not usually show any symptoms; typically being detected for the first time when a fracture occurs. Statistics show that the first fracture doubles the risk of a second fracture—occurring within a year. Fractures are not only painful and reduce the quality of life, but severe hip fractures can also lead to death. Modern sedentary lifestyles contribute to this problem considerably, leading to a much more severe situation for the affected group within the years to come. Osteoporotic hip fractures occur seldom in France, with statistics indicating 8 hip fracture cases among 10,000 people annually. On the other extreme, in Sweden, the amount of osteoporotic hip fractures reaches as high as 20 cases per 10,000 citizens within a year. In the USA, the fracture rate is generally higher and for instance in 2009, the amount of hip fractures per 10,000 cases was 27 and 16 for females and males, respectively [2]. One of the known osteoporosis prevention methods is physical activity. However, more knowledge is needed to determine which types of exercises are the most effective stimulants for bone growth. The base knowledge concerning bone remodeling processes has already been established. It has been shown that inducing high strains in bones can stimulate their growth [3]. On the other hand, high joint loads can lead to osteoarthritis [4]. This leads to the conclusion that establishing an optimum loading scenario could boost bone growth without causing any harm to the joints. Bone strains can be monitored *in vitro* or *in vivo*. Bone strains were measured *in vitro* by a number of researches [5–7]. Unfortunately, cadaver bone studies are limited to the loading conditions that can be replicated in the laboratory. Moreover, usually only a single bone can be tested at a time, since testing the whole complex skeletal system is not feasible in most cases. In addition, accurate muscle forces cannot be applied to cadavers without complex arrangements. *In vivo* studies can be used to circumvent some of the limitations of the *in vitro* studies. *In vivo* studies, see for example [8–11], can be considered more accurate, as the measurements are taken from a living human. However, they raise some ethical concerns due to the invasive methods needed for bone strain measurements. Furthermore, they are limited to superficial bone sites as only those are readily accessible.

The ongoing development of computers and numerical methods has made it possible to model the whole human musculoskeletal system. In early studies, simple finite element models were used to study individual bones [12, 13] and soft tissues. The kinematics and dynamics of the human skeletal system were studied separately by utilizing rigid multibody models [14, 15] with different types of actuators acting as muscles and joints. Nowadays, the computational speed of modern desktop computers allows for the combination of these two approaches in order to achieve a flexible multibody system. Flexible multibody dynamics allows for estimation of joint loads, as well as bone induced strains at any location, thus expanding the possibilities of experimental studies. With the knowledge gathered in experimental studies, new numerical models can be validated and produce reliable results. For example, Al Nazer et al. [16] showed that a shell finite element model of the tibia implemented in multibody simulation can provide sound tibia strain data occurring during human locomotion. In the study, the multibody model results were compared to experimental studies and corresponded well. Also, the computational efficiency of the model showed to be good. Later, a more sophisticated model based on magnetic resonance was presented in [17]. Recently, Kłodowski et al. [18] studied the performance of a full body musculoskeletal system with multiple flexible bone models, showing that the system can be simulated on a desktop computer within several minutes, simultaneously providing strains for four different bones.

In the current paper, the authors combine the knowledge of flexible bone modeling from the finite element method and flexible multibody dynamics. The objective of the current study is to evaluate the strains in the femoral neck using a subject-specific finite element model and flexible multibody model. The finite element model of the femur is analyzed using commercial finite element software to determine the largest load it can endure in the event of a fall concentrated to one side, according to the procedure described in [19]. The test person’s bone can be classified to healthy or osteoporotic groups by comparing the maximum load obtained in the current research to the maximum load results from [19] for healthy and osteoporotic subjects. The flexible multibody model is used to calculate strains within the femoral neck during locomotion. Verification of the flexible multibody model is accomplished with a comparison of simulated ground reaction forces to the forces measured during experimentation. In addition, tensile strains in the proximal lateral aspect of the femur are compared to the in vivo measurements described in [20].

2 Modeling methods

The finite element method and flexible multibody dynamics analysis are used in this study. The static case, which describes the fall-down scenario, is computed using linear finite element formulation and can be expressed as:

$$F = Ku \tag{1}$$

where F is the force vector, K a global stiffness matrix of the finite element model, which is symmetric, and u is the nodal degrees of freedom vector. Nodal degrees of freedom can be divided into the boundary, u_B , and the internal degrees of freedom, u_I . Using the same method, the force vector can be partitioned into support reaction forces, F_R , and externally applied forces, F_E . Correspondingly, (1) can be partitioned as follows:

$$\begin{Bmatrix} F_R \\ F_E \end{Bmatrix} \begin{bmatrix} K_{RB} & K_{RI} \\ K_{EB} & K_{EI} \end{bmatrix} \begin{Bmatrix} u_B \\ u_I \end{Bmatrix} \tag{2}$$

where indices R and E correspond to the rows of the global stiffness matrix associated with reaction forces and externally applied forces. Reaction forces can also be considered as forces resulting from nodal degrees of freedom constrained to zero displacement. Indices B and I denote the columns of the global stiffness matrix that are respectively associated with boundary and internal degrees of freedom. The solution of the system of (2) can be performed in two steps, first solving for the internal degrees of freedom:

$$u_I = K_{EI}^{-1}(F_E - K_{EB}u_B). \tag{3}$$

Finally, solving for reaction forces using the upper part of (2):

$$F_R = \begin{bmatrix} K_{RB} & K_{RI} \end{bmatrix} \begin{Bmatrix} u_B \\ u_I \end{Bmatrix}. \tag{4}$$

The global stiffness matrix can be formulated out of the element stiffness matrices by adding terms that correspond to common degrees of freedom of multiple elements. Linear four-node tetrahedral elements were used in all finite element analyses [21]. The flexible multibody dynamics approach was used to estimate femoral neck strains present during walking. Flexible multibody dynamics is governed by the equation of motion, which can be expressed in the form

$$M\ddot{q} + K_m q + C_q^T \lambda = Q_e + Q_v \tag{5}$$

where M is the mass matrix, K_m the multibody stiffness matrix, q the vector of generalized coordinates, C_q the constraint Jacobian matrix, λ the vector of Lagrange multipliers, and generalized reaction forces are represented by the product $C_q^T \lambda$. Vector Q_e describes the generalized forces, and Q_v is the quadratic velocity vector. The coupling between different bodies is described with algebraic constraint equations:

$$C(q) = 0. \tag{6}$$

Flexible multibody formulation is governed by the set of differential algebraic equations (5) and (6), which are generally time-consuming to solve. In order to avoid supersizing the problem by adding a full finite element representation of flexible bodies, a modal reduction technique is often used as proposed by Agrawal and Shabana [22]. The approach utilized in this study is called component mode synthesis. In this approach, flexible bodies are first represented as finite element models. The finite element representation allows performing constrained modal analysis based on at least two boundary nodes. Deformation modes computed from modal analysis are combined with static correction modes to enrich the database of possible flexible body deformations. This procedure is followed by orthonormalization. Modal matrix, Φ , and modal coordinates, p , are introduced to the multibody formulation instead of the coordinates representing deformation in the body reference system, \bar{u}_f , as shown in (7):

$$\bar{u}_f = \Phi p. \tag{7}$$

Finally, strains can be computed using the strain–deformation relationship [23]:

$$\varepsilon_f = D \bar{u}_f \tag{8}$$

where $\varepsilon_f = [\varepsilon_{11} \ \varepsilon_{22} \ \varepsilon_{33} \ \varepsilon_{12} \ \varepsilon_{13} \ \varepsilon_{23}]^T$ is the elastic strain tensor, and D is a differential operator defined in (9):

$$\varepsilon_{ij} = \frac{1}{2} \left(\bar{u}_{f \ i,j} + \bar{u}_{f \ j,i} + \sum_{k=1}^3 \bar{u}_{f \ k,i} \bar{u}_{f \ k,j} \right). \tag{9}$$

There are several other methods for describing flexible bodies in the multibody formulation [23]; for a comprehensive literature review, see Wasfy and Noor [24].

Estimations for the strains at femoral neck and greater trochanter were performed during walking. In case of the fall-down scenario, strains at the femoral neck were computed as well as the force that is expected to initiate a fracture. The conducted measurements and modeling process are depicted in Fig. 1.

3 The test person and experimental measurements

A clinically healthy 65-year old Caucasian male volunteered for the study. The test person weighs 65 kg and is 168 cm tall. Before measurements, the test person gave written informed consent to the procedures. All experiments were conducted in accordance to the Declaration of Helsinki and with allowance from the local ethical committee of Pirkanmaa hospital district.

In order to reconstruct the geometry and material properties from the test person’s femur, a computed tomography was required. The LightSpeed RT16 scanner from GE Medical System was used for tomography. The slice thickness was set to 0.625 mm, pixel size was 0.3906×0.3906 mm and slice spacing was 0.31 mm. The scan was performed in helical mode to reduce radiation exposure time. Prior to scanning, the scanner was calibrated

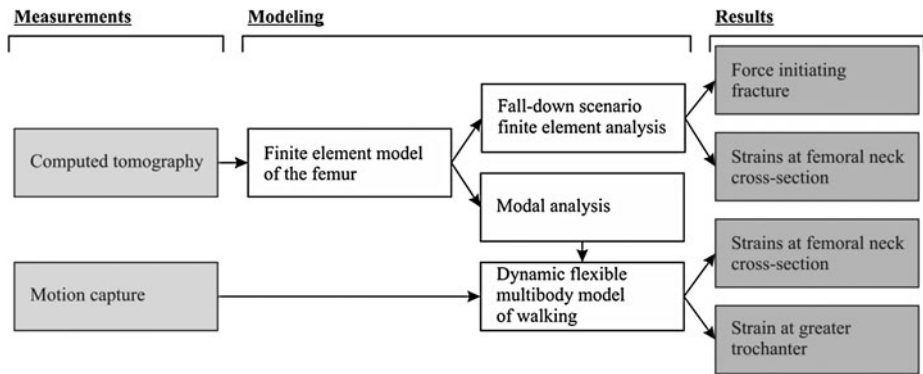


Fig. 1 The research process flow chart

using standard water phantom. Three phantoms made of dipotassium hydrogen phosphate (K_2HPO_4) solutions with concentrations of 100, 200 and 300 mg/cm³ were scanned together with the subject for calibration purposes.

Gait measurements were conducted at the University of Jyväskylä. Two 10-m long force platforms (Raute Inc., Finland) were used to measure the ground reaction forces for both legs independently. The motion was recorded using four high speed cameras (COHU High Performance CCD Camera, San Diego, CA, USA), one placed in front, one behind and two on the side of the test person. Photocell gates were used to initiate and stop measurements synchronously. The subject was dressed in a tightly fitting black matt outfit with 39 passive markers used to track the body segments. The size of the cameras' common field of view restricted the experiment to one full walking cycle. Minimizing the field of view, on the other hand, allows for increasing the precision of the markers' positions acquisition. During the experiment, the test person was instructed to walk barefoot with his usual speed along the force platforms. Four videos recorded during the experiment were digitized using Peak Motus software (ver. 8.1.0, Peak Performance Technologies Inc., USA) to obtain the individual markers' trajectories.

4 Finite element model of femur

A finite element model of the femur was created with the geometry obtained from the computed tomography. Finite element analysis was performed using Ansys (ver. 11, Ansys Inc., Canonsburg, Pennsylvania, USA) software. Linear solid tetrahedral elements [21] were used to discretize the bone. Element size varied from 0.5 to 5 mm, where the smaller elements were used to model cortex at the distal ends of the bone and the larger elements were used to model trabecular bone, as well as cortical bone along the shaft. The model consisted of 331,605 elements based on 1591 sets of material properties. Bone structures were distinguished based on apparent density. Elements covering the volume where the apparent density is above 1400 kg/m³ were considered cortical bone, the elements with apparent density below the threshold were modeled as trabecular bone. Subcortical bone was not considered as a separate structure due to the lack of mathematical dependencies linking material properties and the apparent density or Hounsfield unit scale, which was first introduced by Sir Godfrey Hounsfield in his groundbreaking research on computed tomography [25]. The finite element model is presented in Fig. 2.

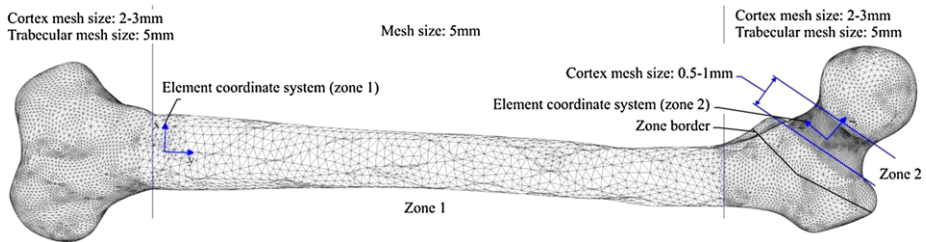


Fig. 2 Finite element model of left femur with indicated mesh sizes and element coordinate systems used to define material properties

Table 1 Material parameters for Young’s modulus equation

	Axis		
	x	y	z
mp_1	0.06	0.51	0.06
mp_2	1.55	1.37	1.51
mp_3	0.0199	0.0225	0.0385
mp_4	18.1	15.5	56.5

Orthotropic material properties were estimated using the relationships between apparent density and other material properties. The apparent density was calculated from the CT voxel values using a linear fit obtained from the densities of the samples scanned together with the test person. Young’s moduli along x -, y - and z -axes were computed according to (10):

$$E_{\text{axis}}(\rho) = \begin{cases} mp_1 \rho^{mp_2} & \rho < T \\ mp_3 \rho - mp_4 & \rho \geq T \end{cases} \quad (10)$$

where mp_1 , mp_2 , mp_3 and mp_4 are parameters, T is the threshold differentiating cortical and trabecular bone and ρ represents the apparent density expressed in $[\text{kg}/\text{m}^3]$. For the trabecular bone the Young’s modulus relationship to density (10) was adopted from Rho et al. [26] and cortical bone material was described utilizing information from Ref. [27]. Threshold T was equal to $1400 \text{ kg}/\text{m}^3$. The material parameters used for Young’s moduli are given in Table 1.

Kirchoff’s moduli in xz -, yz - and zy -planes were assumed to change linearly according to (11):

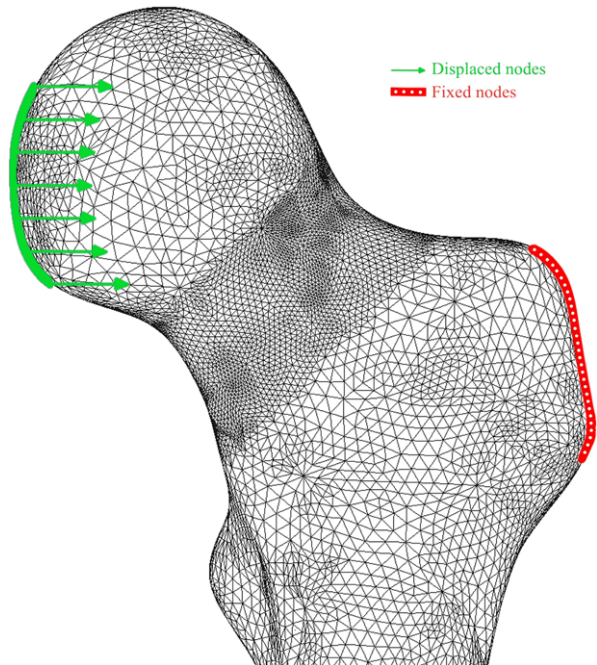
$$G_{\text{plane}}(\rho) = \begin{cases} \frac{mp_5}{19.4} \min(\mathbf{E}_y) & \rho < T \\ mp_6 \rho - mp_7 & \rho \geq T \end{cases} \quad (11)$$

where mp_5 , mp_6 and mp_7 are material parameters, and \mathbf{E}_y represents the vector of all the Young’s moduli in the y -direction for cortical bone. Different fits were used for trabecular and cortical bone [27]. For the trabecular bone, one value was used and corresponds to the lowest elastic modulus in the y -direction within the cortical bone model. The material parameters used for Kirchoff’s moduli are given in Table 2.

Poisson’s ratios were assumed to be 0.3 for all directions [28].

Table 2 Material parameters for Kirchoff's modulus equation

	Plane		
	xz	yz	xy
mp_5	3.81	4.12	4.63
mp_6	0.0054	0.0097	0.0019
mp_7	-5.7553	-12.8309	2.6173

Fig. 3 Boundary conditions of the fall-down scenario finite element model

4.1 Fall-down scenario

A fall onto the greater trochanter is one of the most dangerous scenarios for an osteoporotic femur. Fracture can occur either at the femur [29], most likely in the neck region, or the entire pelvis [2] can be fractured depending on the disease progress in the bones. In order to estimate the maximum impact load that the test person's femoral neck can sustain, a finite element calculation was performed. The test method and bone failure criteria were adopted from [19]. According to the publication, a force causing displacement of 4 % of the initial distance between tip of the femoral head and greater trochanter corresponds to the maximum impact load that the bone can handle. External nodes of the greater trochanter were fixed to provide support. Opposite external nodes on the femoral head were assigned a displacement of 3.3 mm, which corresponds to 4 % of the mentioned distance. Figure 3 illustrates regions where the boundary conditions were applied to the nodes. The model was solved for unknown reaction forces as described in Sect. 2.

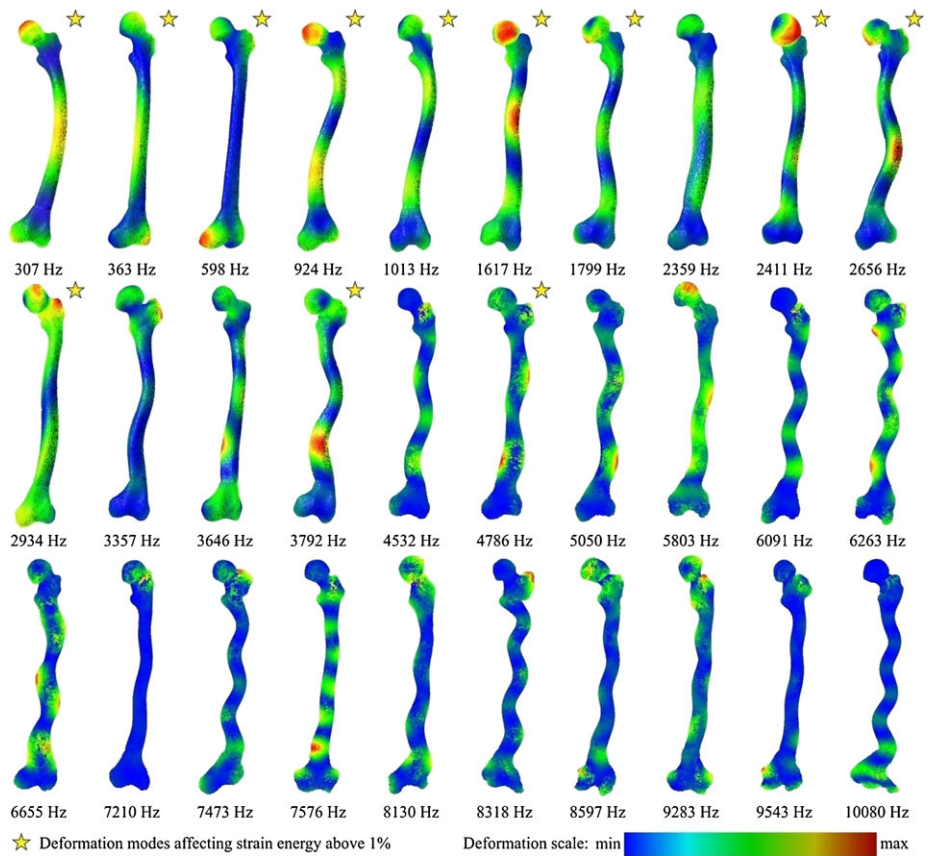


Fig. 4 Craig–Bampton deformation modes for the finite element model of a femur

4.2 Walking: modal analysis

Component mode synthesis uses constrained modal analysis results for flexibility description. In order to perform constrained modal analysis, boundary nodes have to be defined. The boundary nodes should correspond to the fixation points, meaning the nodes at which joints in the multibody formulation are defined. For this reason, two nodes were created at the locations corresponding to the center of the femoral head and the rotation axis of the knee joint. Boundary nodes were connected to the femur’s lower extremity and neck surfaces via rigid massless beam elements. These connections enable application of joint loads to the bone during simulation. The boundary nodes were later used for kinematical connection of the femur to the pelvis and tibia, respectively. For the purpose of describing the flexible femur in multibody simulation, 30 orthonormalized Craig–Bampton [30] deformation modes and corresponding eigenfrequencies were computed. Computation time for the modal analysis was 2.5 hours on a desktop computer with an AMD Phenom II X3 720 (2.8-GHz) processor and 4 GB of RAM. Craig–Bampton deformation modes obtained from the analysis are presented in Fig. 4. Deformation modes affecting strain energy more than 1% are additionally marked with a star.

5 Multibody model of the test person walking

In order to accomplish the specified objective, multibody software is needed. At the time of writing this text, several multibody software platforms were available. Among them: MSC Adams [31], LMS Virtual.Lab [32], Anybody [33], OpenSim [34], VIMS [35]. The last three packages are designed for biomechanical simulations; however, they are intended to work with rigid bodies only. This limits the use of this software in bone strain estimation. To circumvent the problem, the theory of elastodynamics [36] or lumped mass approach [37, 38] could be used. However, these are not state-of-the-art in modeling flexibility of geometrically complex structures. Both MSC Adams and LMS Virtual.Lab allow for modeling of general flexible bodies. However, modeling of human musculoskeletal systems is extremely laborious, due to the number of complex components and models of substructures. Combining MSC Adams and LifeMOD software packages gives flexibility for general multibody code and at the same time provides tools for human modeling.

MSC Adams (ver. R3, MSC software corporation, Santa Ana, California, USA) general multibody package [31] was chosen as the simulation environment. Human musculoskeletal modeling was performed using the dedicated LifeMOD (ver. 1.0.0, LifeModeler Inc., San Clemente, California, USA) plug-in. A three-dimensional skeletal model of the test person was created based on five parameters: weight, height, age, ethnicity and gender. To fully represent the subject, the model was further adjusted using the measurement of joint locations from the computed tomography scans. The model is depicted in Fig. 5. After this adjustment, kinematical joint descriptions were introduced and passive recording muscle representations were added.

Marker trajectories obtained from the experiment were used to drive the model in the inverse dynamics, producing the desired muscle length change patterns. These are used by the muscle controller in forward dynamics. The simulation time step was 0.01 seconds and a contact optimized integrator was chosen. After inverse dynamics simulation, the rigid left femur was replaced with a flexible one, generated in Ansys. Passive muscles were replaced with active muscles controlled via PID (proportional-integral-derivative) controllers with contraction splines obtained from the inverse dynamics. Foot–ground contact model was based on spherical elements that were added: one at the heel, one in the middle of each foot, and one under each phalanx. Penalty contact formulation with friction was used to describe the foot–ground contact. The principle of the contact formulation is presented in Fig. 6.

During the simulation, the contact is detected when the contact ellipse penetrates the contact plane. Normal reaction force, F_n , is then computed using equation

$$F_n = K d^n + C(d)d \quad (12)$$

where d is the penetration depth, n the exponent, K the contact stiffness and $C(d)$ the damping coefficient depending on the damping depth (14). Friction force, F_f , is computed using Coulomb's model:

$$F_f = \mu F_n \quad (13)$$

where μ is the coefficient of friction. The contact damping coefficient is computed using (14), where c_{\max} is the maximum damping coefficient and d_{\max} is the maximum penetration depth [39]:

$$C(d) = \begin{cases} \left(\frac{\sin\left(\frac{d}{d_{\max}} \cdot \pi - \frac{\pi}{2}\right)}{2} + 0.5 \right) \cdot c_{\max} & d \leq d_{\max} \\ c_{\max} & d > d_{\max} \end{cases} \quad (14)$$

Fig. 5 Multibody model used in walking simulation

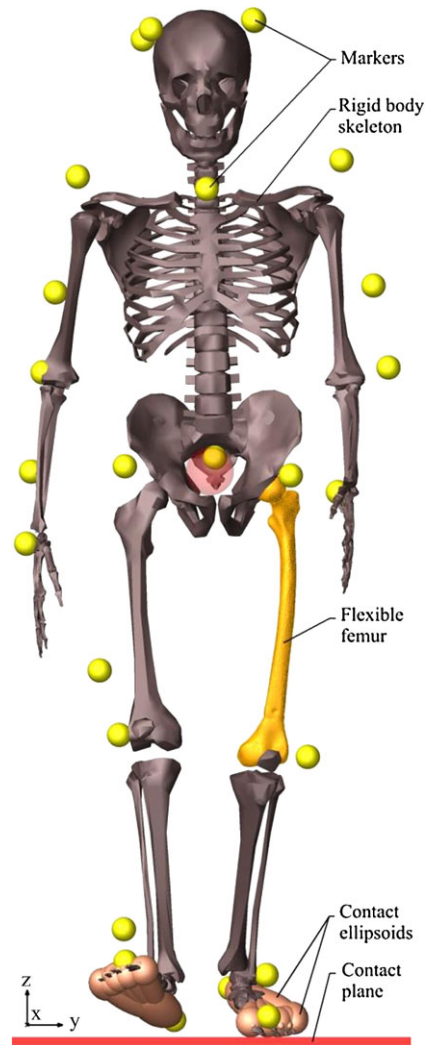
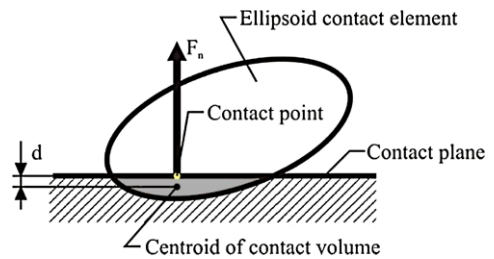


Fig. 6 Ellipsoid-solid penalty contact formulation



Initial contact parameters were adopted from [40]. Through an iterative optimization process, where the stability of the model was used as the target function, the final contact stiffness was determined to be 300 N/mm, maximum damping was 25 N s/mm, exponent n

was equaled to 1 and the maximum penetration depth was constrained to 0.01 mm. Due to the static nature of friction between bare feet and the force platforms, the friction coefficient was set to 1. Walking speed was determined from the inverse dynamics and used as the initial condition for the forward dynamics simulation. The forward dynamics simulation was performed to obtain femoral strains during locomotion. The same time step and integrator settings were used as for the inverse dynamics.

During the forward dynamics simulation, the model is only driven by muscles; to maintain vertical stability the LifeMOD tracking agent is used. In case of the presented model, only torques are applied to the center of mass of the model to prevent the model from falling down. As mentioned in previous publications [18], the stabilization procedure does not influence the simulation results in a considerable manner.

Inclusion of the full finite element model to the multibody simulation would increase the computational time remarkably. To circumvent this problem, modal reduction [30] of the finite element model is applied. Modal representation of the bone model allows for a decrease in the size of the system from over 196,000 variables to 30 modal coefficients, which specify the contribution of each of the modes. It is important to keep in mind that the flexible model has to be solved for each time step, thus reduction of the model size is a necessity. A single deformation mode describes the deformed state of all the nodes in the finite element model under a certain loading condition. This technique is based on the assumption that using a sufficient amount of deformation modes and computing weighted averages of the modes, one can obtain the deformation of the body, closely matching the result of the complete finite element model.

6 Results

The finite element fall-down scenario computation produced a total support force equal to 14.6 kN. This force represents the maximum impact force according to the test procedure described in [19]. According to the procedure, 4 % displacement of the femoral neck will correspond to the fracture condition. The normal strains around the cross section of the femoral neck obtained in the finite element analysis are presented in Fig. 7. Strains were computed at the same nodes in the finite element analysis as in the flexible multibody simulation to allow a direct comparison of the results. All figures related to locomotion represent averaged results of two gait cycles. The timescale of the plots is scaled in percentage of

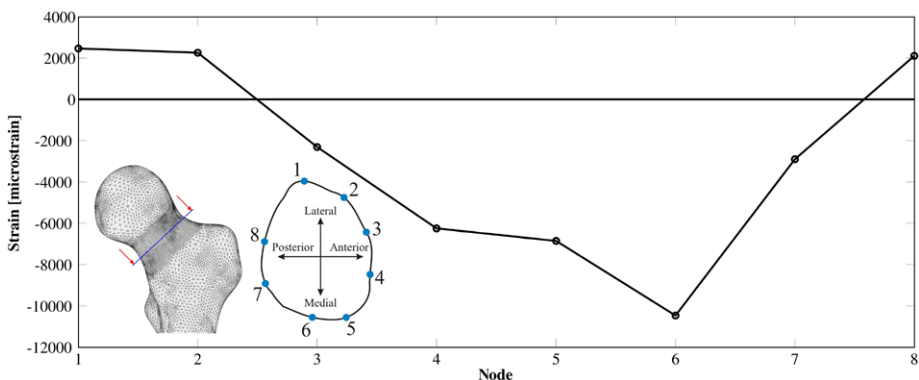


Fig. 7 Normal strains at femoral neck during fall-down scenario

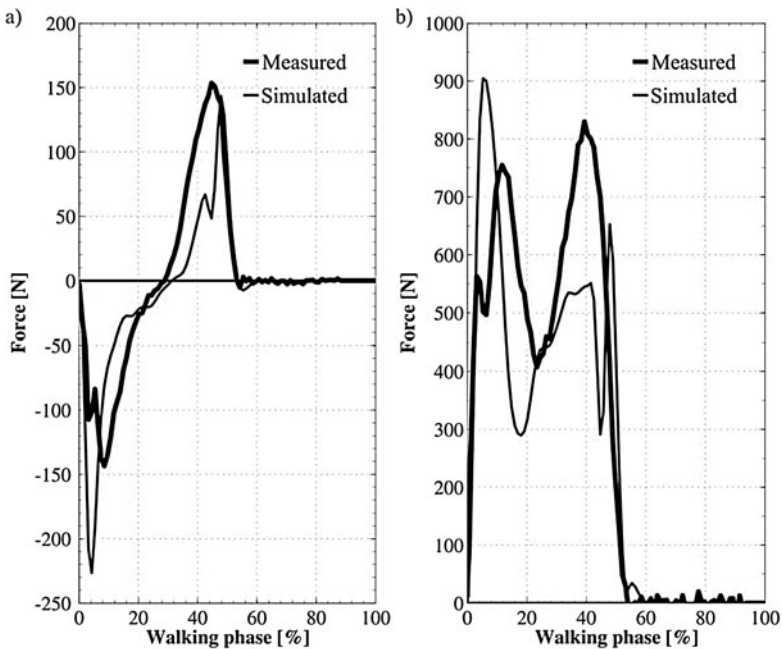


Fig. 8 Horizontal (a) and vertical (b) components of ground reaction force measured during walking experiment and obtained from multibody simulation

walking phase, where 0 % corresponds to heel strike, 53.5 % to toe-off and 100 % is the end of the forward swing of the leg. Ground reaction forces obtained from the measurements and multibody simulation are presented in Fig. 8 for model verification. The horizontal component of the ground reaction force (Fig. 8a) is a result of the friction between foot and the force platform. Strain results were obtained at eight external nodes located around the femoral neck's middle cross section. The strains were computed along the axis perpendicular to the cross section as indicated in Fig. 9. Figure 10 illustrates axial strains at the proximal lateral aspect of the femur; the location of the node and axis along which the strains were computed correspond to Ref. [20].

7 Discussion and conclusions

Finite element analysis of the fall-down scenario according to the procedure described in [19] showed, as expected, that the test person is not likely to have osteoporosis. The classification is based on the values for healthy and osteoporotic test subjects reported in [19]. The span of results reported in the cited study is 2.5 to 15 kN for healthy subjects and 1.9 to 8 kN for subjects with osteoporosis. The impact force result of 14.6 kN is above one standard deviation from the average results obtained from the healthy subjects in Orwoll's study [19], and this allows for the classification of the test person as not belonging to the high-risk hip fracture group. The force is also larger in value than the largest result of osteoporotic subject in Orwoll's study [19] which makes it very unlikely for the subject to have symptoms of osteoporosis. The age of the test person is 8 years less than the average age of

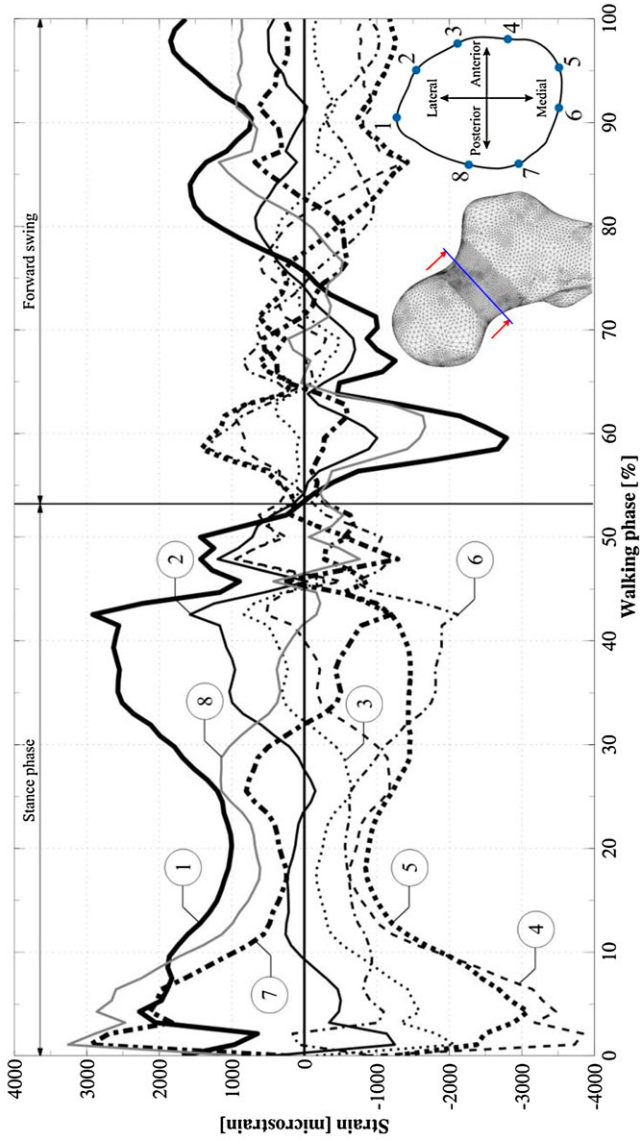
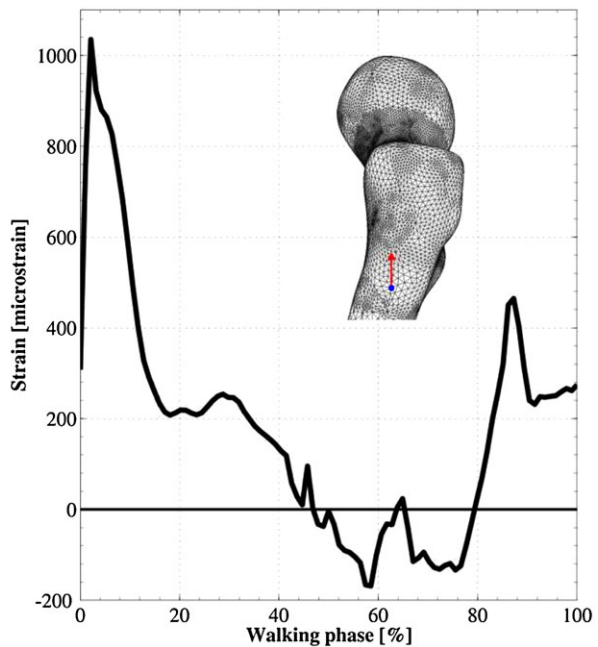


Fig. 9 Axial strains around middle femoral neck cross section obtained from multibody simulation of walking

Fig. 10 Axial strains at the proximal lateral aspect of the femur during walking obtained from multibody simulation. Node location is indicated by a *dot* and the axis orientation is shown by an *arrow*



the subjects in Orwoll's research and explains the greater bone strength results. Figure 7 indicates bending combined with compression as the dominating deformation mode during the fall-down scenario test, which is in line with the referenced study. The highest compressive strains occur at the medial aspect of the femoral neck and reach a value of -10467μ . This is approximately 5 times larger than the strain at this location during walking and 2.5 times larger than the largest compressive strain in the chosen femoral neck cross section during walking. In [29] de Bakker et al. based on their high-speed camera studies on the mechanism of proximal femur fractures suggest that the failure process is in fact a two-stage process, where the failure initiates in the superior surface and later on in the inferior part of the femoral neck. Their study supports the importance of reporting compressive strains, while it was hypothesized that the detailed failure mechanism may actually be associated with buckling—occurring in the superior region due to the large compressive stress.

Multibody simulation showed strain results at the lateral aspect of the femur that compare well with the data obtained in the *in vivo* study by Aamodt et al. [20]. These results are shown in Fig. 10. Peak strain is achieved at heel strike, and in the current simulation it reaches 1023μ . The Aamodt et al.'s study indicated a maximum value of 1300μ for the heel strike. Stance phase, as cited in study [20], is characterized by moderate tensile strains and the forward swing oscillates between compressive and tensile loading within the range of -400 to 200μ . In the current study, swing phase strains vary between -168 and 464μ , which is in good agreement with the cited results. The overall correlation between current strain results and results from Aamodt et al. [20] is evaluated to be on the level of 67%. The difference is caused mostly by age and gender differences between test persons in the studies; however, due to the similar neck-shaft angles (129° —in current study, and 124° —in [20]) and the same activity, it is assumed that the comparison is relevant. Comparing correlation of Aamodt et al.'s separate walking cycles to the average cycle, the correlation was around 94%. Thus, even for the same subject quite a large variation of the walking cycle is possible. Summarizing the strain results from the current study with those from the

experimental research, it is observed that the zero-strain level in the experimental study is shifted by approximately $+200 \mu$ with respect to the current research. This could clearly reduce the correlation between studies.

The horizontal component of the ground reaction force (Fig. 8a) obtained in the simulation shows 85 % correlation when compared to measurements, which is a fairly good result. The vertical component of the ground reaction force (Fig. 8b) presents satisfactory correlation with the measurements with a correlation factor of 83 %. It is noted that the vertical component of the ground reaction force is overestimated in the simulation during the heel strike, while during the push-off phase, this force is underestimated. Comparison of the extreme strain span at the heel strike with the same quantity at the push-off phase shows a 26 % difference. At the same time the vertical component of the ground reaction force decreased by 39 %. This suggests that the sensitivity of the femoral neck strains to ground reaction force is moderate. Nevertheless, more detailed sensitivity analysis is needed to quantify the femoral neck strain to ground reaction force relationship. The discrepancies can be caused by the stabilization agent's need to maintain an upright position for the model. However, energy applied by the stabilization system did not account for more than 5 % of the total kinetic energy at any time step.

The most interesting results from the simulation are the strains in the femoral neck. This relatively small cross section of the largest human bone is subject to relatively large strains even during walking. The vertical component of the hip joint reaction at peak reaches 236 % of body weight during heel strike. In average, during the stance phase, hip joint load is around 110 % of the body weight, while during the forward swing this value drops to 70 % of the body weight.

The loading state is complex, it combines compression and bending, thus both tensile and compressive strains can be seen in Fig. 9. During the stance phase, the largest strains are transmitted through the femoral neck. Correlation between the shape of strain curves and the ground reaction force can be seen from a comparison of the vertical ground reaction force (Fig. 8b) and the femoral neck strains (Fig. 9). Two characteristic peaks corresponding to heel strike and push-off phase can be seen. The highest absolute strains can be observed during the heel strike due to the impact. Forward swing is characterized by strains not exceeding 50–60 % of the stance phase strains. The stance phase loads mostly occur from the body mass and from rapid deceleration on the heel strike and from the change of force related to the push-off phase. Loads during forward swing come from the inertia of the whole leg and muscle forces created by muscles linking the femur and pelvis. The beginning of the forward swing is characterized by a change in bending direction, the antero-medial aspect of the femoral neck starts to transmit compressive load and the postero-lateral section takes the tensile load. The situation inverts around the middle of the forward swing, changing to a tensile-compressive load division in the same fashion as in the stance phase. Stance phase is characterized by bending combined with compressive strains, which is reasonable due to the body weight support. Forward swing phase is almost entirely loaded by pure bending. The results show that flexible multibody dynamics can be used to evaluate femoral neck strains reliably.

Finally, limitations of the current study need to be presented. Previous research done on the influence of the loading direction on the proximal femur fracture using finite element method has shown that the loading direction has a substantial influence on the fracture load magnitude [41]. In the current study, the fracture load was determined based on the method used in the in vitro study conducted by Orwoll and only considered one loading direction. This clearly limits the conclusions that can be drawn from the results.

Multibody simulation presented in this paper is based on commercial software. The biggest unknown is the muscle control system implemented in LifeMOD. LifeMOD uses

the PID control mechanism to compute muscular forces, as well as allowing for the introduction of maximum force production constrains for each muscle individually. However, load division between muscles within the same muscle group is calculated through a closed code optimization routine. The muscle force solver used in the LifeMOD is based on the research conducted by Crowninshield and Brand [42]. While in their study the mathematical model was capable of producing muscle activity patterns in agreement with the observed activity patterns of the muscles determined by electromyography, the LifeMOD muscle force solver still lacks sound validation. For this reason, the strain results presented in this paper represent one possible output for the specific subject and physical activity. As the muscle redundancy problem can be solved in a number of ways, the strain result output can also vary for a single subject. And more research needs to be done in order to specify the upper and lower strain limits, which can be observed at specific bone sites.

In order to obtain strain results for specific motion produced by the test person, muscle forces would have to be reproduced from the experiment in the model. Accomplishing this task is still challenging, as direct muscle force measurement is not feasible without surgical intervention and indirect force measurement based on electromyography has a downside of not always being reliable in terms of electromyography–force relationship [43]. Furthermore, the electromyography signals are not obtainable from all of the muscles, due to difficulties in accessing them. On the other hand, the use of electromyography as an additional input for muscle optimization procedure is a promising technique [44].

Stabilization of the body during walking is another issue that needs to be addressed. At the current development stage, posture stabilization is maintained by applying external forces at the body center of mass by LifeMOD tracking agent. Even though the energy introduced by the external forces to the system is relatively small (1–5 %), those forces do not have any real equivalents. Desirably, they should be replaced by a more sophisticated balancing system, which would utilize only muscles to compensate for any balancing problems. The skeletal model used in the simulation is based on the LifeMOD anthropometric database which is based on US army survey [45]. The model was scaled using the test person anthropometric data and kinematical joint locations. The lower extremities were adjusted with care based on the computed tomography. While the geometrical properties and mass distribution of the femur are as accurate as possible within the used measurement method, the same does not apply for the other parts of the skeletal model that are derived from the database. The use of anthropometric database with scaling instead of detailed subject-specific measurements can lead to errors in the simulated muscle forces and ground reaction force, as is shown in the sensitivity analysis done by Dao et al. [46].

Future investigations will be directed towards alleviating the limitations of the currently presented models. In addition, establishing a suitable link between the two models presented in the paper will allow studying the effects of the loading direction, protective nature of the soft tissues, and contact surface materials by utilizing the contact forces calculated when using the multibody model as an input in the detailed finite element model of the femur. Eventually, after careful validation of the models and the approach, this procedure could be used to estimate the strains and stresses occurring in the whole hip area under different falling down scenarios and to develop protective equipment for elderly people to prevent bone fractures.

References

1. International Osteoporosis Foundation: Osteoporosis in Europe: Indicators of Progress and Outcomes from the European Parliament Osteoporosis Interest Group and European Union Os-

- teoporosis Consultation Panel Meeting (2004). <http://www.iofbonehealth.org/download/osteofound/filemanager/publications/pdf/eu-report-2005.pdf>
2. Nieves, J., Bilezikian, J., Lane, J., Einhorn, T., Wang, Y., Steinbuch, M., Cosman, F.: Fragility fractures of the hip and femur: incidence and patient characteristics. *Osteoporos. Int.* **21**(3), 399–408 (2010)
 3. Turner, C.H.: Three rules for bone adaptation to mechanical stimuli. *Bone* **23**, 399–407 (1998)
 4. Arokoski, J.P., Jurvelin, J.S., Väättäinen, U., Helminen, H.J.: Normal and pathological adaptations of articular cartilage to joint loading. *Scand. J. Med. Sci. Sports* **10**(4), 186–198 (2000)
 5. Sharkey, N.A., Hamel, A.J.: A dynamic cadaver model of the stance phase of gait: performance characteristics and kinetic validation. *Clin. Biomech.* **13**(6), 420–433 (1998)
 6. Guterla, C.C., Gardner, T.R., Rajanb, V., Ahmadv, C.S., Hunga, C.T., Ateshian, G.A.: Two-dimensional strain fields on the cross section of the human patellofemoral joint under physiological loading. *J. Biomech.* **42**(9), 1275–1281 (2009)
 7. Peterman, M.M., Hamel, A.J., Cavanagh, P.R., Piazza, S.J., Sharkey, N.A.: In vitro modeling of human tibial strains during exercise in micro-gravity. *J. Biomech.* **34**(5), 693–698 (2001)
 8. Lanyon, L.E., Hampson, W.G.J., Goodship, A.E., Shah, J.S.: Bone deformation recorded in vivo from strain gauges attached to the human tibial shaft. *Acta Orthop. Scand.* **46**, 256–268 (1975)
 9. Burr, D.B., Milgrom, C., Fyhrie, D., Forwood, M., Nyska, M., Finestone, A., Hoshaw, S., Saiag, E., Simkin, A.: In vivo measurement of human tibial strains during vigorous activity. *Bone* **18**(5), 405–410 (1996)
 10. Hoshaw, S.J., Fyhrie, D.P., Takano, Y., Burr, D.B., Milgrom, C.: A method suitable for in vivo measurement of bone strain in humans. *J. Biomech.* **30**(5), 521–524 (1997)
 11. Milgrom, C., Finestone, A., Benjoyan, N., Simkin, A., Ekenman, I., Burr, D.B.: Measurement of strain and strain rate developed by jumping exercises in vivo in humans. In: *Proceedings of Southern Biomedical Engineering Conference*, p. 108 (1998)
 12. Dujovne, A., Wevers, H.W.: Experimental measurements of proximal tibial displacements under load: comparison with FE models. *J. Biomech.* **22**(10), 1006 (1989)
 13. Marom, S.A., Linden, M.J.: Computer aided stress analysis of long bones utilizing computed tomography. *J. Biomech.* **23**(5), 399–404 (1990)
 14. Hof, A.L.: An explicit expression for the moment in multibody systems. *J. Biomech.* **25**(10), 1209–1211 (1992)
 15. Soutas-Little, R.W., Lovasik, K.A., Krueger, M.: Multibody systems analysis of above-knee prostheses to permit rapid gait (racewalking). *Adv. Bioeng.* **20**, 543–546 (1991)
 16. Al Nazer, R., Rantalainen, T., Heinonen, A., Sievänen, H., Mikkola, A.: Flexible multibody simulation approach in the analysis of tibial strain during walking. *J. Biomech.* **41**(5), 1036–1043 (2008)
 17. Al Nazer, R., Klodowski, A., Rantalainen, T., Heinonen, A., Sievänen, H., Mikkola, A.: Analysis of dynamic strains in tibia during human locomotion based on flexible multibody approach integrated with magnetic resonance imaging technique. *Multibody Syst. Dyn.* **20**(4), 287–306 (2008)
 18. Klodowski, A., Rantalainen, T., Mikkola, A., Heinonen, A., Sievänen, H.: Flexible multibody approach in forward dynamic simulation of locomotive strains in human skeleton with flexible lower body bones. *Multibody Syst. Dyn.* **25**(4), 395–409 (2011)
 19. Orwoll, E., Marshall, L., Nielson, C., Cummings, R., Lapidus, S.J., Cauley, J.A., Ensrud, K., Lane, N., Hoffmann, P.R., Kopperdahl, D.L., Keaveny, T.M.: Finite element analysis of the proximal femur and hip fracture risk in older men. *J. Bone Miner. Res.* **24**(3), 475–483 (2009)
 20. Aamodt, A., Lund-Larsen, J., Eine, J., Andersen, E., Benum, P., Schnell Husby, O.: In vivo measurements show tensile axial strain in the proximal lateral aspect of the human femur. *J. Orthop. Res.* **15**(6), 927–931 (1997)
 21. ANSYS, Inc., ANSYS® Academic Research, Release 11.0, Help System, Element Reference (2007)
 22. Agrawal, O.P., Shabana, A.A.: Dynamic analysis of multibody systems using component modes. *Comput. Struct.* **21**(6), 1303–1312 (1985)
 23. Shabana, A.A.: *Dynamics of Multibody Systems*, 3rd edn., p. 374. Cambridge University Press, New York (2005)
 24. Wasfy, T.M., Noor, A.K.: Computational strategies for flexible multibody systems. *Appl. Mech. Rev.* **56**(6), 553–613 (2003)
 25. Hounsfield, G.N.: Computerized transverse axial scanning (tomography). Part 1. Description of system. *Br. J. Radiol.* **46**, 1016–1022 (1973)
 26. Rho, J.Y., Hobatho, M.C., Ashman, R.B.: Relations of mechanical properties to density and CT numbers in human bone. *Med. Eng. Phys.* **17**(5), 347–355 (1995)
 27. Espinoza Oriaz, A.A., Deuerling, J.M., Landrigan, M.D., Renaud, E., Roeder, R.K.: Anatomic variation in the elastic anisotropy of cortical bone tissue in the human femur. *J. Mech. Behav. Biomed. Mater.* **2**(3), 255–263 (2009)

28. Van Rietbergen, B., Odgaard, A., Kabel, J., Huiskes, R.: Direct mechanics assessment of elastic symmetries and properties of trabecular bone architecture. *J. Biomech.* **29**(12), 1653–1657 (1996)
29. de Bakker, P.M., Manske, S.L., Ebacher, V., Oxland, T.R., Cripton, P.A., Guy, P.: During sideways falls proximal femur fractures initiate in the superolateral cortex: evidence from high-speed video of simulated fractures. *J. Biomech.* **42**(12), 1917–1925 (2009)
30. Craig, R.R., Bampton, M.C.C.: Coupling of substructures for dynamic analysis. *AIAA J.* **6**(7), 1313–1319 (1968)
31. MSC.Software, MSC.ADAMS®, Release R3, Help System (2008)
32. LMS Engineering Innovation. LMS Virtual. Lab (2011). <http://www.lmsintl.com/virtuallab>
33. Damsgaard, M., Rasmussen, J., Christensen, S.T., Surma, E., de Zee, M.: Analysis of musculoskeletal systems in the AnyBody modeling system. *Simul. Model. Pract. Theory* **14**(8), 1100–1111 (2006)
34. Delp, S.L., Anderson, F.C., Arnold, A.S., Loan, P., Habib, A., John, C.T., Guendelman, E., Thelen, D.G.: OpenSim: open-source software to create and analyze dynamic simulations of movement. *Biomed. Eng.* **54**(11), 1940–1950 (2007)
35. Chao, E., Armiger, R., Yoshida, H., Lim, J., Haraguchi, N.: Virtual interactive musculoskeletal system (VIMS) in orthopaedic research, education and clinical patient care. *J. Orthop. Surg. Res.* **2**(1), 2–21 (2007)
36. Erdman, A.G., Sandor, G.N.: Kineto-elastodynamics—a review of the state of the art trends. *Mech. Mach. Theory* **7**(1), 19–33 (1972)
37. Kamman, J.W., Huston, R.L.: Multibody dynamics modeling of variable length cable systems. *Multibody Syst. Dyn.* **5**(3), 211–221 (2001)
38. Raman-Nair, W., Baddour, R.E.: Three-dimensional dynamics of a flexible marine riser undergoing large elastic deformations. *Multibody Syst. Dyn.* **10**(4), 393–423 (2003)
39. C. U. Biomechanics Research Group Inc. LifeMOD online user's manual (2008). http://www.lifemodeler.com/LM_Manual_2008/
40. Gilchrist, L.A., Winter, D.A.: A two-part, viscoelastic foot model for use in gait simulations. *J. Biomech.* **29**(6), 795–798 (1996)
41. Wakao, N., Harada, A., Matsui, Y., Takemura, M., Shimokata, H., Mizuno, M., Ito, M., Matsuyama, Y., Ishiguro, N.: The effect of impact direction on the fracture load of osteoporotic proximal femurs. *Med. Eng. Phys.* **31**(9), 1134–1139 (2009)
42. Crowninshield, R.D., Brand, R.A.: A physiologically based criterion of muscle force prediction in locomotion. *J. Biomech.* **14**(11), 793–801 (1981)
43. Rantalainen, T., Klodowski, A., Piitulainen, H.: Effect of innervation zones in estimating biceps brachii force-EMG relationship during isometric contraction. *J. Electromyogr. Kinesiol.* **22**(1), 80–87 (2012)
44. Amarantini, D., Rao, G., Berton, E.: A two-step EMG-and-optimization process to estimate muscle force during dynamic movement. *J. Biomech.* **43**(9), 1827–1830 (2010)
45. Gordon, C.C., Churchill, T., Clauser, C.E., Bradtmiller, B., McConville, J.T., Tebbets, I., Walker, R.A.: Anthropometric survey of U.S. army personnel, methods and summary statistics (1989)
46. Dao, T.T., Marin, F., Ho Ba Tho, M.C.: Sensitivity of the anthropometrical and geometrical parameters of the bones and muscles on a musculoskeletal model of the lower limbs. In: 31st Annual International Conference of the IEEE EMBS, Minneapolis, Minnesota, USA, September 2–6, pp. 5251–5254 (2009)